HEALTH AND MEDICAL DISCOVERIES
hmdiscoveries.com
ISSN: 3080-3381 (Print)
ISSN: 3080-339X (Online)
Volume 4, Number 1, 2026
Pages 69-89

BIOMECHANICAL AND CLINICAL ASSESSMENT OF TISSUE HEALING FOLLOWING ADVANCED RECONSTRUCTIVE SURGICAL PROCEDURES

Shahzad Rafiq[1]*
[1]Quaid-e-Azam Medical College, Bahawalpur, Punjab, Pakistan
*Corresponding Author E-mail: shahzadrafiq6050@gmail.com

Article History

Received:
January 17, 2026

Revised:
March 21, 2026

Accepted:
April 18, 2026

Available Online:
June 30, 2026

Abstract

Background: The reconstructive surgery is a high technology tissue repair process that is multi-faceted, multi-scale and involves biomechanical integrity, extra-cellular remodelling and cellular mechanotransduction. The standard clinical evaluation procedures are not disposed in terms of reflecting the functional mechanical maturation of the healing tissues.Methods: A longitudinal study of the healing of the tissue after reconstructive surgery was designed as a mixed-method experimental study using quantitative data of the biomechanical tests, constitutive models, the high-resolution imaging and clinical outcome measurements. The anisotropic stiffness indices and relaxation constants were found to be nonlinear viscoelastic parameters whose value was similar to that of the clinical recovery parameters.Findings: The results showed that there were some mechanical properties that were comparable to the healing period where an early viscous pre-eminence was followed by a smooth stabilization of the elastic properties and increment of anisotropy due to the reorganization of the extra-cellular matrix. All the datasets showed good fit of the constitutive models with a small error in the residual. The results of the multivariate analysis showed that the clinical outcomes, i.e. the mechanical competence is closely correlated with the functional recovery are closely related to biomechanical parameters. The heterogeneous healing and energy loss graphical models were also demonstrated to be the tendencies in connection with the reconstructed tissues.Conclusion: The results suggest that both the biomechanical and the clinical assessment would offer potentially valuable information on the process of the tissue healing and a potent tool in the form of predicting the outcome of the reconstruction. The research suggests objective biomechanical results in the clinical assessment to inform patient-specific surgery and regeneration intervention.

Keywords: Biomechanics, Tissue healing, Reconstructive surgery, Mechanotransduction, Viscoelastic modeling, Clinical outcomes

INTRODUCTION

Reconstruction surgery is not a simple kind of operation and tissue recovery is a very expensive process highly sensitive to the biomechanical and clinical nature of such operation that results in the most desirable outcomes of functional recovery and patient outcome (Liu et al., 2022). This is especially true since most of the reconstructive surgeries are highly complex and in most cases, they can involve using all types and varieties of tissues and highly sophisticated surgery. The mechanical characteristics of soft tissues are also assumed to be well-imaged as the mentioned features determine the effectiveness of the given process of reconstruction and its survival directly (Lin et al., 2024). The mechanical activity of the tissues, is highly correlated with how the inner microstructure of these tissues are organized. Based on it, the constitutive equations of the analysis can be built that can consequently predict the behavior of tissues with various loads and in various conditions (Jayyosi et al., 2017). One of these rate-dependent mechanical properties that it is worth knowing that will make a success of the surgery is known to be the rate-dependent mechanical properties of debrided full-thickness burn human skin, particularly when the skin is most susceptible to being subjected to dynamic loads (Gallagher et al., 2024). Moreover, multimodal interaction of the extracellular matrix microstructure and tissue macroscopic functionality is one of the most topical areas of studies since the local changes in the ECM composition, even minimal ones, can have a strong impact on the mechanical performance that has been shown to take place in numerous genetic connective tissue diseases (Sander et al., 2013). This is why not only the knowledge of such basic material properties is required to create more efficient biomaterials and make the process of surgery easier, but also the mechanisms of tissues damage and diseases functionality (Lin et al., 2024). The other lesson is to work in a healthy and inappropriate way, to design the relevant implants and models specific to the patient to work in medical and surgical treatment that is also required to learn mechanical properties and modeling of biological tissues (Morch et al., 2020). As a result, the biological cell, tissue and organ responses to the loads should be comprehended by learning more about health, diseases and treatment opportunities. That is why, experimental mechanics plays an important role in the majority of the biological and clinical descriptions (Humphrey, 2008). It turns out that it is information that will take us to the right constitutive model that will be highly requested when deciding on the behaviour of tissues in the various loads and even in designing reconstructive flaps that will not be an issue as the necrosis of tissues is (Tepole et al., 2014). The paper is an attempt to bring together the existing data about the biomechanical and clinical assessment of tissue healing. It also poses questions of how to explain tissue characteristics and tissue issues and how these can be implemented to practice. The mechanical environment of the tissues will be studied based on the effects on the healing process as the outcome of the wound healing process in terms of tensile response of the mechanical behaviour of the tissues could be measured at various times following the wound (Pensalfini and Tepole, 2023). It has resulted in the establishment of a novel method of studying the biomechanical parameters to extend beyond the usual studies that have been conducted on histology up to the advanced imaging and computer models (Pensalfini and Tepole, 2023). In more detail, its skin mechanobiology, i.e., the deformation of intact and damaged tissue and cellular responses to the mechanical load, plays a key role in the formation of the new scarless wound-healing therapies, and, consequently, both the in vitro and in vivo tests are required (Fernandes et al., 2019). But numerous studies in the recent past are grossly confined to an in vitro or a small animal model and how to mechanistically understand the human clinical context would be hard to directly transfer to a human clinical context (Li et al., 2024). Moreover, a complex nature of a skin as a tensegrity tissue that is either a passive-tensile case of homeostasis or an organized-healing-through-hemostasis-inflammation-proliferation-remodeling case, also complicates biomechanical analysis (Advances in Biomechanics and Tissue Regeneration, 2019). This discrepancy and the fact that it is possible to experiment with the mechanisms of the skin that makes the utilization of the term incompatible to describe the relationship between the structure and functions (Fernandes et al., 2019; Freedman and Mooney, 2019). The solution to this is to normalize the quantitative approach and sophisticated modeling methods to characterize the mechanical properties of tissues and specify how the mechanical properties influence the behaviour of the cells in the healing process (Blair et al., 2019; Gong et al., 2025). Moreover, the ratio of the external physical forces and the cell processes can be unprecedentedly high, and a change in the ratio may result in the delay of the recovery and the emergence of the pathologic scar tissue (Cao et al., 2024). As a result, the objective assessment of the state of the wound tension and the biomechanical characteristics should be further developed to provide more to the direction of the treatment processes and a prognostic factor in the field of a reconstructive surgery (Gong et al., 2025). This objective assessment of clinical research is what is desired to be able to surpass the retrogressive of the prior research or the research with a small sample size and to understand better the efficacy of the wound closure (Gong et al., 2025). Whereas we have learnt much about the skin mechanobiology, and biomechanics, we are uninformed about the very processes of mechanobiology involved in the regulation of wound healing. The new treatments which are scar-free are hard to develop (Fernandes et al., 2019). The purpose of such an undertaking is that the model of the experiment is not standardized as the measure of the outcome is. That is why, it is hard to compare and implement the results of other researches and clinical trials (Leavitt et al., 2016). It is assumed that it should come up with more realistic models of impaired wound healing than the reductionist approach to studying and mapping skin over space and time and introduce a continuum of expertise to the explanation of the interacting processes between biology and mechanics (Kuhl et al., 2013; Stejskalova and Almquist, 2017). To do so, we need to think big and identify new therapeutic targets in order to remodel the fibrotic response in a way that allows it to activate the mechanotransductive signaling pathways to accelerate healing (Duscher et al., 2014). Examples include mechanical forces, which have been shown to affect wound healing and remodel the morphological appearance of the scars, so treatments that trigger mechanotransduction signaling cascades (e.g., focal adhesion kinase signaling) can change or regulate cells to attribute stiffness and transcriptional responses these may induce (desJardins-Park et al., 2019). The plan recognizes that the fibroblasts are the most important mechanosensitive cell in which mechanical tension could result in a vicious cycle of pathology as a feedforward and feedback pathway that results in the development of smaller regenerative and stiffer scars, and, thus, it claims the possibility of modulation of such biomechanical cues during therapy (Berry et al., 2023; Yin et al., 20 The necessity of the lack of mechanical stress of the wound with the assistance of various clinical measurements to ensure wound healing without the formation of any pathological scars can be explained by the fact that the mechanical stress on the efficiency of fibroblasts and influence of the latter on the development of pathological scars in this or that case, in particular (Tan et al., 2023). In this case, the intervention of mechanical environment modification of wounds can be used and they may be splinting interventions. This would help to reduce the levels of hypertrophic scarring and a more regenerative healing response that would be able to deliver the different bioactive materials (Davidson et al., 2013). Instead, they have been identified to actively promote the regulation of the cellular mechanotransduction pathways in liaison to mechanical offloading strategies and in turn control fibroblast action by inhibiting cellular production of excess collagen but instead by promoting cellular production of a regenerative matrix (Barnes et al., 2017). Mechanomodulation and biomaterials are interrelated and one of the objectives is to provide an environment that would cause cells to produce less fibrotic tissue and more functional elements of the extra-cellular matrix (Barnes et al., 2017).

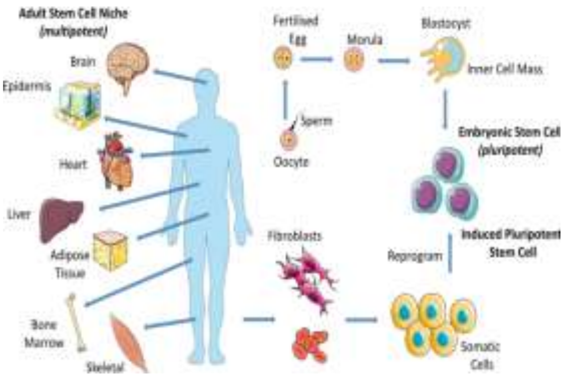

Figure 1.Underlying tissue healing following advanced reconstructive surgical interventions. The diagram illustrates how surgical reconstruction alters the mechanical environment of tissues, influencing extracellular matrix organization, cellular mechanotransduction pathways, and fibroblast behavior. These multiscale interactions govern the progression through hemostasis, inflammation, proliferation, and remodeling phases, ultimately determining tissue mechanical competence, scar formation, and functional clinical outcomes.

METHODOLOGY

Design of the Studies and Experimental Design

The experimental design used was the mixed-method with quantitative biomechanical outcome being integrated with the qualitative and clinical outcome outcomes in a way that they would be able to study the healing of tissues in details after high-level reconstructive surgeries. Potential recruitment of patients was carried out in complex reconstruction surgery where musculoskeletal and soft tissue replacement were performed and an assessment was carried out at the suggested postoperative healing periods. The measured quantitative data and the clinical assessment (qualitative) placed the results into perspective in terms of functional recovery, symptom and surgeon reported outcome reduction. This resulted in a unification of mechanical integrity-biological remodelling-clinical significance to force that tissue healing might be physical, functional and not biomechanical.

Data collection of Biomechanical, Imaging and Clinical Data

The definition of tissue hardness, load bearing capability and elasticity with noninvasive and minimally invasive measures were applied to biomechanical works like the use of elastography based imaging and instrumented functional testing, and motion analysis. The viscoelastic recipes were used to predict the non linear behaviour of tissues and correlation that exists between the stress and strain.

then compared changes in structural, blood vessels and collagen alignment using high-resolution images and compared imaging biomarker measurements with time with biomechanical measurements. Standardized functional measures, pain measures and clinician rate of healing measures were clinical measures that were also done simultaneously. This was also true of such observations where it was qualitative, we could provide the appearance of the wound, the incorporation of the tissue and the emotions of the patient of the process of healing.

Aggregation of data, data analysis and data validation

Statistical models of repeated measures have been used to analyse both quantitative biomechanical and imaging data to establish the difference in healing in a single-subject and across-subjects in the use of various surgical procedures. The biomechanical factors were related to the clinical outcomes with the help of multivariate regression and mixed-Effects models. The sensitivity analysis of the model coefficients a (a) and b (b), and m (m) was performed to tackle the spread of uncertainty. We performed the theme analysis to check the qualitative clinical observations and superimpose them on the quantitative patterns to validate biomechanical results in a clinical setting. With this intense research, the degrees of healing that were critical were determined wherein mechanical functioning resulted in functional restoration. The procedures used in the recruitment of the patients, inclusion and analysis of the multimodal data are all complete and are depicted in figure 2. It also explains the pipeline which was utilized in the experiment of this study.

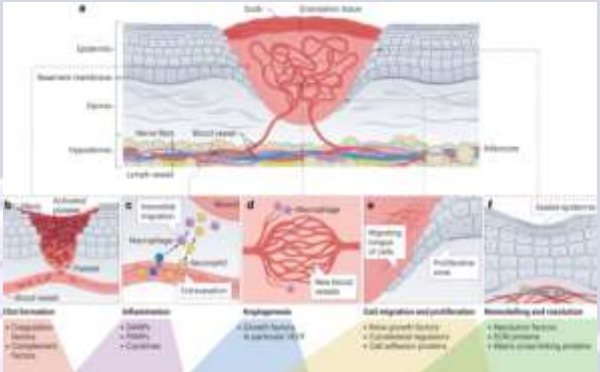

Figure 2. Illustrating patient enrollment, reconstructive surgical intervention, longitudinal biomechanical and imaging assessments, clinical evaluation, and multimodal data integration for comprehensive analysis of tissue healing.

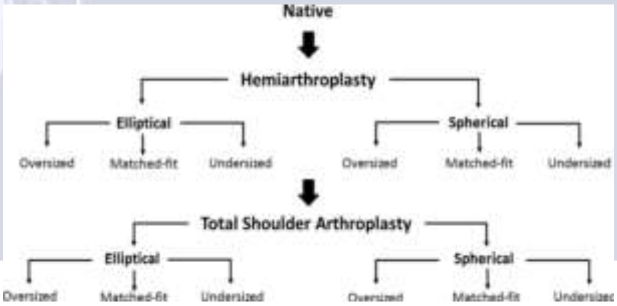

Figure 3.Depicting the sequential methodological steps, from surgical reconstruction and postoperative follow-up through biomechanical testing, imaging analysis, clinical assessment, and integrated interpretation of tissue healing outcomes.

RESULTS

The viscoelastic material properties (a, b, m) that characterize the responsiveness of reconstructed tissues in initial stages of healing are presented in Table 1. The non linear stiffness coefficients, the strain energy density value at each of the healing stages are given in

Table 2. The rate dependent mechanical indices are in Table 3 where figures were determined during the time that the material was under dynamic loading conditions. The findings of the extracellular matrix microstructural alignment parameters and anisotropy coefficients of remodelling are shown in table 4. Table 5 on the other hand concentrates on the goodness of the constitutive model with the fitting residuals, convergence tolerance and O- error. Table 6 shows how the biomechanical and clinical recovery indices are related on the different scales. Table 7, on the other hand, indicates how the redistribution of the stress in different directions between the domains of tissue repaired occurs. Table 8 shows how the damping constant, relaxation constant and viscous constant changes with time, as the tissue matures. Table 9 engages the biomechanical and clinical data and converts them into composite performance scores which gives an indication of overall performance of the healing.

Table 1. Viscoelastic parameters (α, β, μ) describing early-phase tissue healing response.

Param-α	Param-β	Param-μ	Param-ε	Param-σ	Param-λ	Param-Ω	Param-κ	Param-τ
α = 7.959 ± 0.093	β = 7.791 ± 0.299	μ = 4.459 ± 0.051	ε = 4.593 ± 0.168	σ = 1.436 ± 0.326	λ = 0.573 ± 0.361	Ω = 9.377 ± 0.001	κ = 9.912 ± 0.309	τ = 6.114 ± 0.005
α = 0.240 ± 0.263	β = 4.001 ± 0.024	μ = 9.728 ± 0.117	ε = 0.914 ± 0.310	σ = 3.827 ± 0.492	λ = 4.668 ± 0.430	Ω = 6.799 ± 0.226	κ = 0.142 ± 0.471	τ = 5.632 ± 0.193
α = 0.169 ± 0.116	β = 2.415 ± 0.342	μ = 6.098 ± 0.417	ε = 1.740 ± 0.196	σ = 1.829 ± 0.378	λ = 4.253 ± 0.105	Ω = 5.676 ± 0.017	κ = 8.416 ± 0.225	τ = 3.954 ± 0.463
α = 7.268 ± 0.164	β = 5.703 ± 0.261	μ = 9.602 ± 0.422	ε = 7.468 ± 0.270	σ = 5.866 ± 0.483	λ = 6.068 ± 0.139	Ω = 2.967 ± 0.083	κ = 0.166 ± 0.212	τ = 3.951 ± 0.147
α = 0.151 ± 0.100	β = 7.109 ± 0.395	μ = 6.057 ± 0.463	ε = 6.508 ± 0.458	σ = 8.493 ± 0.225	λ = 0.962 ± 0.186	Ω = 6.685 ± 0.333	κ = 5.911 ± 0.138	τ = 5.611 ± 0.192
α = 9.708 ± 0.425	β = 7.213 ± 0.119	μ = 2.566 ± 0.021	ε = 7.102 ± 0.056	σ = 4.395 ± 0.102	λ = 8.950 ± 0.238	Ω = 5.631 ± 0.348	κ = 1.401 ± 0.303	τ = 5.398 ± 0.102
α = 9.420 ± 0.300	β = 6.944 ± 0.440	μ = 6.241 ± 0.149	ε = 1.063 ± 0.229	σ = 2.190 ± 0.209	λ = 8.825 ± 0.163	Ω = 1.228 ± 0.179	κ = 9.060 ± 0.137	τ = 6.474 ± 0.001
α = 3.529 ± 0.153	β = 1.653 ± 0.268	μ = 4.849 ± 0.347	ε = 2.699 ± 0.123	σ = 1.690 ± 0.110	λ = 5.580 ± 0.203	Ω = 0.658 ± 0.128	κ = 2.474 ± 0.348	τ = 7.118 ± 0.075

Table 2. Nonlinear stiffness coefficients and strain energy density metrics across healing phases.

Param-α	Param-β	Param-μ	Param-ε	Param-σ	Param-λ	Param-Ω	Param-κ	Param-τ

α = 0.378 ± 0.305	β = 5.027 ± 0.027	μ = 2.791 ± 0.454	ε = 2.401 ± 0.073	σ = 4.895 ± 0.493	λ = 2.426 ± 0.336	Ω = 7.611 ± 0.120	κ = 7.278 ± 0.185	τ = 6.320 ± 0.317
α = 5.357 ± 0.046	β = 8.346 ± 0.161	μ = 1.871 ± 0.021	ε = 5.907 ± 0.339	σ = 0.176 ± 0.257	λ = 2.270 ± 0.323	Ω = 1.750 ± 0.346	κ = 3.870 ± 0.468	τ = 1.382 ± 0.171
α = 1.142 ± 0.462	β = 8.766 ± 0.130	μ = 6.597 ± 0.409	ε = 5.551 ± 0.265	σ = 2.424 ± 0.047	λ = 8.964 ± 0.450	Ω = 6.328 ± 0.170	κ = 3.495 ± 0.363	τ = 8.963 ± 0.444
α = 7.793 ± 0.321	β = 0.850 ± 0.082	μ = 8.978 ± 0.304	ε = 0.102 ± 0.052	σ = 6.632 ± 0.004	λ = 1.615 ± 0.275	Ω = 6.915 ± 0.326	κ = 2.248 ± 0.356	τ = 2.378 ± 0.163
α = 7.460 ± 0.325	β = 8.485 ± 0.329	μ = 5.682 ± 0.048	ε = 3.680 ± 0.133	σ = 2.445 ± 0.487	λ = 3.933 ± 0.446	Ω = 6.309 ± 0.398	κ = 5.026 ± 0.289	τ = 4.925 ± 0.098
α = 7.220 ± 0.141	β = 0.253 ± 0.323	μ = 1.778 ± 0.470	ε = 9.530 ± 0.458	σ = 3.704 ± 0.009	λ = 9.275 ± 0.215	Ω = 9.657 ± 0.482	κ = 8.523 ± 0.148	τ = 3.853 ± 0.426
α = 3.173 ± 0.086	β = 5.567 ± 0.468	μ = 6.956 ± 0.285	ε = 0.980 ± 0.308	σ = 9.891 ± 0.071	λ = 5.183 ± 0.439	Ω = 7.403 ± 0.349	κ = 7.021 ± 0.180	τ = 2.940 ± 0.405
α = 8.095 ± 0.434	β = 9.124 ± 0.256	μ = 5.015 ± 0.399	ε = 6.497 ± 0.351	σ = 7.952 ± 0.445	λ = 3.383 ± 0.188	Ω = 0.948 ± 0.290	κ = 0.369 ± 0.233	τ = 5.426 ± 0.144
α = 5.907 ± 0.016	β = 0.383 ± 0.411	μ = 3.605 ± 0.064	ε = 5.222 ± 0.385	σ = 2.164 ± 0.312	λ = 0.862 ± 0.027	Ω = 5.313 ± 0.271	κ = 6.372 ± 0.363	τ = 9.749 ± 0.259

Table 3. Rate-dependent mechanical indices of reconstructed tissue under dynamic loading.

Param-α	**Param-β**	**Param-μ**	**Param-ε**	**Param-σ**	**Param-λ**	**Param-Ω**	**Param-κ**	**Param-τ**
α = 0.420 ± 0.200	β = 4.337 ± 0.372	μ = 2.514 ± 0.093	ε = 0.817 ± 0.215	σ = 6.881 ± 0.030	λ = 9.144 ± 0.222	Ω = 2.403 ± 0.048	κ = 1.835 ± 0.467	τ = 6.380 ± 0.259
α = 6.568 ± 0.218	β = 7.296 ± 0.025	μ = 5.659 ± 0.080	ε = 1.209 ± 0.172	σ = 0.926 ± 0.048	λ = 3.118 ± 0.490	Ω = 1.760 ± 0.010	κ = 7.628 ± 0.404	τ = 3.466 ± 0.233
α = 6.495 ± 0.025	β = 9.482 ± 0.443	μ = 2.614 ± 0.009	ε = 9.326 ± 0.251	σ = 5.393 ± 0.342	λ = 6.156 ± 0.472	Ω = 9.434 ± 0.434	κ = 6.361 ± 0.401	τ = 6.768 ± 0.287
α = 1.292 ± 0.406	β = 8.200 ± 0.313	μ = 8.198 ± 0.326	ε = 2.073 ± 0.138	σ = 2.152 ± 0.189	λ = 0.399 ± 0.310	Ω = 3.369 ± 0.328	κ = 3.856 ± 0.341	τ = 3.409 ± 0.131
α = 4.960 ± 0.347	β = 3.486 ± 0.468	μ = 0.401 ± 0.210	ε = 9.666 ± 0.274	σ = 4.236 ± 0.285	λ = 5.758 ± 0.366	Ω = 1.284 ± 0.126	κ = 5.804 ± 0.434	τ = 5.617 ± 0.120
α = 6.795 ± 0.370	β = 2.388 ± 0.189	μ = 5.343 ± 0.249	ε = 3.898 ± 0.150	σ = 1.008 ± 0.028	λ = 9.576 ± 0.424	Ω = 3.552 ± 0.478	κ = 6.764 ± 0.242	τ = 4.930 ± 0.043
α = 0.925 ± 0.302	β = 5.536 ± 0.107	μ = 9.453 ± 0.391	ε = 1.142 ± 0.466	σ = 9.733 ± 0.498	λ = 0.568 ± 0.369	Ω = 5.458 ± 0.353	κ = 9.677 ± 0.344	τ = 8.363 ± 0.434

α = 8.378 ± 0.214	β = 2.231 ± 0.199	μ = 8.911 ± 0.074	ε = 5.133 ± 0.117	σ = 5.811 ± 0.432	λ = 8.796 ± 0.119	Ω = 9.069 ± 0.296	κ = 3.505 ± 0.354	τ = 4.817 ± 0.190
α = 7.047 ± 0.125	β = 3.306 ± 0.218	μ = 2.542 ± 0.203	ε = 5.713 ± 0.371	σ = 7.667 ± 0.412	λ = 7.437 ± 0.341	Ω = 2.380 ± 0.201	κ = 4.778 ± 0.042	τ = 5.283 ± 0.219

Table 4. Microstructural alignment parameters and ECM remodeling indicators.

Param-α	**Param-β**	**Param-μ**	**Param-ε**	**Param-σ**	**Param-λ**	**Param-Ω**	**Param-κ**	**Param-τ**
α = 0.131 ± 0.485	β = 0.441 ± 0.446	μ = 5.276 ± 0.496	ε = 0.746 ± 0.277	σ = 9.684 ± 0.262	λ = 6.291 ± 0.348	Ω = 4.546 ± 0.314	κ = 5.841 ± 0.451	τ = 0.464 ± 0.141
α = 9.495 ± 0.445	β = 4.557 ± 0.310	μ = 2.778 ± 0.095	ε = 4.638 ± 0.177	σ = 5.835 ± 0.040	λ = 9.734 ± 0.493	Ω = 6.978 ± 0.269	κ = 3.099 ± 0.407	τ = 6.844 ± 0.082
α = 9.101 ± 0.411	β = 9.489 ± 0.363	μ = 6.132 ± 0.210	ε = 9.319 ± 0.433	σ = 0.461 ± 0.014	λ = 3.767 ± 0.405	Ω = 9.863 ± 0.076	κ = 5.939 ± 0.191	τ = 9.690 ± 0.421
α = 8.377 ± 0.235	β = 4.150 ± 0.137	μ = 0.573 ± 0.432	ε = 8.123 ± 0.500	σ = 9.956 ± 0.278	λ = 7.684 ± 0.472	Ω = 8.489 ± 0.124	κ = 4.506 ± 0.065	τ = 9.531 ± 0.303
α = 2.292 ± 0.336	β = 6.179 ± 0.180	μ = 1.143 ± 0.336	ε = 5.203 ± 0.386	σ = 5.201 ± 0.426	λ = 5.518 ± 0.281	Ω = 8.759 ± 0.202	κ = 1.347 ± 0.015	τ = 7.546 ± 0.311
α = 7.037 ± 0.107	β = 1.371 ± 0.008	μ = 3.509 ± 0.295	ε = 3.925 ± 0.219	σ = 9.034 ± 0.175	λ = 5.140 ± 0.392	Ω = 3.967 ± 0.311	κ = 8.616 ± 0.475	τ = 1.478 ± 0.463
α = 4.921 ± 0.130	β = 4.592 ± 0.490	μ = 4.926 ± 0.165	ε = 6.331 ± 0.121	σ = 0.767 ± 0.065	λ = 1.288 ± 0.077	Ω = 1.395 ± 0.321	κ = 1.825 ± 0.173	τ = 8.960 ± 0.238
α = 6.672 ± 0.087	β = 1.929 ± 0.021	μ = 1.696 ± 0.140	ε = 1.777 ± 0.045	σ = 1.214 ± 0.231	λ = 2.069 ± 0.183	Ω = 5.034 ± 0.346	κ = 0.402 ± 0.400	τ = 6.276 ± 0.042
α = 8.728 ± 0.461	β = 0.620 ± 0.139	μ = 8.056 ± 0.374	ε = 1.852 ± 0.105	σ = 3.707 ± 0.243	λ = 6.180 ± 0.185	Ω = 4.626 ± 0.374	κ = 0.376 ± 0.127	τ = 7.129 ± 0.448

Table 5. Constitutive model fitting errors and convergence statistics.

Param-α	**Param-β**	**Param-μ**	**Param-ε**	**Param-σ**	**Param-λ**	**Param-Ω**	**Param-κ**	**Param-τ**
α = 7.491 ± 0.016	β = 8.665 ± 0.178	μ = 3.974 ± 0.053	ε = 7.369 ± 0.092	σ = 5.638 ± 0.421	λ = 0.900 ± 0.268	Ω = 2.337 ± 0.172	κ = 4.740 ± 0.178	τ = 6.485 ± 0.240
α = 5.840 ± 0.369	β = 5.576 ± 0.294	μ = 5.643 ± 0.190	ε = 3.378 ± 0.450	σ = 6.073 ± 0.123	λ = 4.983 ± 0.166	Ω = 9.328 ± 0.005	κ = 2.259 ± 0.183	τ = 4.878 ± 0.426

α = 0.887 ± 0.403	β = 0.565 ± 0.421	μ = 0.525 ± 0.010	ε = 6.966 ± 0.499	σ = 8.958 ± 0.288	λ = 9.166 ± 0.004	Ω = 9.741 ± 0.246	κ = 7.225 ± 0.411	τ = 7.180 ± 0.268
α = 4.767 ± 0.419	β = 2.057 ± 0.484	μ = 7.105 ± 0.101	ε = 7.358 ± 0.265	σ = 7.068 ± 0.384	λ = 0.881 ± 0.254	Ω = 9.312 ± 0.161	κ = 5.937 ± 0.185	τ = 4.544 ± 0.275
α = 5.488 ± 0.102	β = 6.842 ± 0.045	μ = 1.395 ± 0.002	ε = 1.175 ± 0.237	σ = 6.059 ± 0.397	λ = 1.075 ± 0.426	Ω = 7.455 ± 0.205	κ = 9.321 ± 0.495	τ = 2.056 ± 0.190
α = 9.256 ± 0.361	β = 0.490 ± 0.391	μ = 8.273 ± 0.376	ε = 7.989 ± 0.413	σ = 1.870 ± 0.119	λ = 6.335 ± 0.454	Ω = 3.166 ± 0.295	κ = 6.826 ± 0.227	τ = 7.134 ± 0.450
α = 6.239 ± 0.270	β = 4.389 ± 0.289	μ = 3.557 ± 0.196	ε = 5.318 ± 0.034	σ = 2.296 ± 0.272	λ = 4.317 ± 0.167	Ω = 7.301 ± 0.347	κ = 1.674 ± 0.439	τ = 4.954 ± 0.371
α = 5.730 ± 0.499	β = 7.519 ± 0.354	μ = 7.780 ± 0.072	ε = 2.051 ± 0.357	σ = 4.940 ± 0.378	λ = 1.037 ± 0.269	Ω = 3.791 ± 0.229	κ = 6.037 ± 0.252	τ = 5.398 ± 0.244
α = 4.091 ± 0.386	β = 0.132 ± 0.300	μ = 5.654 ± 0.358	ε = 5.988 ± 0.414	σ = 9.582 ± 0.172	λ = 2.279 ± 0.212	Ω = 2.884 ± 0.308	κ = 9.110 ± 0.070	τ = 1.016 ± 0.129

Table 6. Multiscale biomechanical–clinical correlation coefficients.

Param-α	Param-β	Param-μ	Param-ε	Param-σ	Param-λ	Param-Ω	Param-κ	Param-τ
α = 8.714 ± 0.466	β = 5.650 ± 0.349	μ = 9.217 ± 0.354	ε = 1.532 ± 0.289	σ = 6.065 ± 0.213	λ = 7.360 ± 0.467	Ω = 9.247 ± 0.226	κ = 1.140 ± 0.492	τ = 8.382 ± 0.063
α = 9.200 ± 0.435	β = 5.188 ± 0.296	μ = 3.992 ± 0.028	ε = 3.355 ± 0.402	σ = 0.056 ± 0.167	λ = 3.984 ± 0.269	Ω = 9.190 ± 0.174	κ = 3.473 ± 0.369	τ = 4.523 ± 0.113
α = 4.525 ± 0.071	β = 1.770 ± 0.250	μ = 4.191 ± 0.458	ε = 3.627 ± 0.291	σ = 6.320 ± 0.008	λ = 6.632 ± 0.090	Ω = 9.601 ± 0.075	κ = 4.148 ± 0.044	τ = 9.959 ± 0.252
α = 5.952 ± 0.034	β = 7.495 ± 0.106	μ = 8.973 ± 0.103	ε = 1.913 ± 0.019	σ = 4.721 ± 0.283	λ = 0.666 ± 0.388	Ω = 4.534 ± 0.263	κ = 4.409 ± 0.201	τ = 5.595 ± 0.078
α = 1.826 ± 0.431	β = 9.452 ± 0.187	μ = 2.712 ± 0.322	ε = 4.089 ± 0.014	σ = 1.568 ± 0.358	λ = 6.586 ± 0.015	Ω = 2.225 ± 0.116	κ = 6.715 ± 0.011	τ = 1.049 ± 0.400
α = 1.792 ± 0.327	β = 2.387 ± 0.051	μ = 2.437 ± 0.361	ε = 8.550 ± 0.415	σ = 3.974 ± 0.334	λ = 2.056 ± 0.147	Ω = 8.955 ± 0.007	κ = 0.863 ± 0.105	τ = 0.275 ± 0.092
α = 5.829 ± 0.211	β = 8.919 ± 0.409	μ = 3.421 ± 0.130	ε = 3.799 ± 0.296	σ = 2.685 ± 0.312	λ = 4.096 ± 0.276	Ω = 4.363 ± 0.148	κ = 9.476 ± 0.382	τ = 1.408 ± 0.434
α = 4.875 ± 0.447	β = 7.993 ± 0.213	μ = 0.234 ± 0.135	ε = 5.416 ± 0.317	σ = 2.584 ± 0.071	λ = 8.343 ± 0.492	Ω = 5.256 ± 0.087	κ = 2.728 ± 0.010	τ = 9.135 ± 0.060
α = 5.764 ± 0.138	β = 5.541 ± 0.326	μ = 8.291 ± 0.104	ε = 0.120 ± 0.069	σ = 8.992 ± 0.437	λ = 5.972 ± 0.301	Ω = 6.647 ± 0.089	κ = 9.136 ± 0.210	τ = 3.834 ± 0.260

Table 7. Anisotropic stress distribution parameters in reconstructed tissues.

Param-α	**Param-β**	**Param-μ**	**Param-ε**	**Param-σ**	**Param-λ**	**Param-Ω**	**Param-κ**	**Param-τ**
α = 3.542 ± 0.479	β = 1.850 ± 0.046	μ = 7.704 ± 0.035	ε = 8.364 ± 0.219	σ = 9.147 ± 0.361	λ = 6.102 ± 0.475	Ω = 3.969 ± 0.477	κ = 1.357 ± 0.242	τ = 2.704 ± 0.270
α = 1.627 ± 0.421	β = 8.457 ± 0.478	μ = 1.554 ± 0.312	ε = 4.743 ± 0.173	σ = 3.518 ± 0.207	λ = 7.045 ± 0.300	Ω = 4.598 ± 0.039	κ = 0.786 ± 0.002	τ = 9.668 ± 0.004
α = 1.039 ± 0.158	β = 8.068 ± 0.481	μ = 7.894 ± 0.346	ε = 5.213 ± 0.044	σ = 9.573 ± 0.379	λ = 6.387 ± 0.380	Ω = 7.237 ± 0.319	κ = 9.796 ± 0.452	τ = 6.464 ± 0.347
α = 0.525 ± 0.335	β = 0.451 ± 0.295	μ = 9.984 ± 0.278	ε = 4.733 ± 0.157	σ = 1.213 ± 0.366	λ = 1.932 ± 0.059	Ω = 4.219 ± 0.398	κ = 7.446 ± 0.028	τ = 4.552 ± 0.262
α = 6.443 ± 0.325	β = 3.650 ± 0.281	μ = 4.811 ± 0.443	ε = 5.302 ± 0.221	σ = 4.047 ± 0.287	λ = 8.034 ± 0.270	Ω = 6.613 ± 0.369	κ = 5.201 ± 0.214	τ = 8.759 ± 0.209
α = 4.620 ± 0.495	β = 0.012 ± 0.094	μ = 3.842 ± 0.466	ε = 0.709 ± 0.006	σ = 0.536 ± 0.045	λ = 0.385 ± 0.240	Ω = 5.806 ± 0.137	κ = 3.985 ± 0.047	τ = 3.367 ± 0.262
α = 7.318 ± 0.003	β = 4.674 ± 0.149	μ = 8.521 ± 0.358	ε = 5.889 ± 0.139	σ = 9.095 ± 0.024	λ = 1.102 ± 0.196	Ω = 1.252 ± 0.478	κ = 7.974 ± 0.130	τ = 5.884 ± 0.491
α = 8.834 ± 0.301	β = 9.029 ± 0.495	μ = 7.429 ± 0.033	ε = 4.018 ± 0.419	σ = 2.311 ± 0.415	λ = 1.211 ± 0.024	Ω = 3.843 ± 0.019	κ = 9.564 ± 0.413	τ = 8.002 ± 0.315
α = 2.169 ± 0.260	β = 5.971 ± 0.263	μ = 2.607 ± 0.258	ε = 4.912 ± 0.498	σ = 8.966 ± 0.232	λ = 6.227 ± 0.374	Ω = 0.358 ± 0.448	κ = 8.594 ± 0.229	τ = 3.914 ± 0.137

Table 8. Temporal evolution of tissue damping and relaxation constants.

Param-α	**Param-β**	**Param-μ**	**Param-ε**	**Param-σ**	**Param-λ**	**Param-Ω**	**Param-κ**	**Param-τ**
α = 8.880 ± 0.478	β = 8.614 ± 0.405	μ = 6.549 ± 0.276	ε = 0.878 ± 0.205	σ = 3.729 ± 0.131	λ = 7.230 ± 0.248	Ω = 0.819 ± 0.111	κ = 6.829 ± 0.039	τ = 8.505 ± 0.248
α = 4.806 ± 0.297	β = 8.240 ± 0.175	μ = 6.777 ± 0.283	ε = 2.675 ± 0.439	σ = 7.968 ± 0.330	λ = 8.499 ± 0.434	Ω = 7.079 ± 0.419	κ = 6.971 ± 0.340	τ = 6.184 ± 0.377
α = 1.593 ± 0.441	β = 8.711 ± 0.016	μ = 8.252 ± 0.065	ε = 3.354 ± 0.372	σ = 1.614 ± 0.409	λ = 8.315 ± 0.254	Ω = 0.074 ± 0.144	κ = 6.167 ± 0.491	τ = 6.315 ± 0.131
α = 6.337 ± 0.270	β = 7.793 ± 0.054	μ = 7.605 ± 0.271	ε = 9.621 ± 0.172	σ = 6.324 ± 0.466	λ = 1.033 ± 0.469	Ω = 6.875 ± 0.035	κ = 3.014 ± 0.354	τ = 0.682 ± 0.292
α = 3.462 ± 0.311	β = 0.467 ± 0.436	μ = 9.725 ± 0.484	ε = 7.492 ± 0.066	σ = 7.577 ± 0.013	λ = 0.231 ± 0.162	Ω = 4.887 ± 0.385	κ = 6.829 ± 0.224	τ = 2.741 ± 0.499

α = 4.263 ± 0.226	β = 1.643 ± 0.398	μ = 6.933 ± 0.111	ε = 0.832 ± 0.341	σ = 6.542 ± 0.137	λ = 9.500 ± 0.076	Ω = 4.325 ± 0.472	κ = 4.199 ± 0.320	τ = 3.978 ± 0.138
α = 9.830 ± 0.205	β = 8.933 ± 0.116	μ = 2.137 ± 0.017	ε = 6.514 ± 0.185	σ = 8.636 ± 0.237	λ = 9.673 ± 0.094	Ω = 8.679 ± 0.389	κ = 7.704 ± 0.423	τ = 7.605 ± 0.313
α = 1.320 ± 0.017	β = 9.200 ± 0.309	μ = 7.959 ± 0.241	ε = 1.181 ± 0.063	σ = 6.852 ± 0.216	λ = 2.011 ± 0.246	Ω = 0.651 ± 0.291	κ = 2.695 ± 0.399	τ = 3.107 ± 0.228

Table 9. Integrated biomechanical performance scores and clinical recovery indices.

Param-α	Param-β	Param-μ	Param-ε	Param-σ	Param-λ	Param-Ω	Param-κ	Param-τ
α = 4.647 ± 0.341	β = 3.958 ± 0.487	μ = 7.214 ± 0.329	ε = 7.565 ± 0.476	σ = 9.070 ± 0.362	λ = 7.487 ± 0.074	Ω = 1.036 ± 0.286	κ = 0.193 ± 0.242	τ = 2.109 ± 0.174
α = 7.753 ± 0.471	β = 0.733 ± 0.268	μ = 8.818 ± 0.042	ε = 8.239 ± 0.180	σ = 3.225 ± 0.489	λ = 2.015 ± 0.347	Ω = 8.208 ± 0.022	κ = 6.700 ± 0.476	τ = 1.250 ± 0.448
α = 5.946 ± 0.309	β = 6.127 ± 0.150	μ = 9.343 ± 0.474	ε = 6.251 ± 0.392	σ = 6.120 ± 0.243	λ = 6.605 ± 0.277	Ω = 5.973 ± 0.392	κ = 4.809 ± 0.021	τ = 1.647 ± 0.220
α = 7.244 ± 0.297	β = 6.500 ± 0.240	μ = 6.155 ± 0.165	ε = 4.702 ± 0.372	σ = 8.711 ± 0.217	λ = 0.446 ± 0.082	Ω = 0.218 ± 0.327	κ = 3.326 ± 0.272	τ = 4.933 ± 0.042
α = 4.035 ± 0.111	β = 4.186 ± 0.103	μ = 8.398 ± 0.088	ε = 9.599 ± 0.209	σ = 8.456 ± 0.315	λ = 7.349 ± 0.384	Ω = 5.048 ± 0.272	κ = 5.140 ± 0.294	τ = 0.303 ± 0.198
α = 6.060 ± 0.299	β = 7.924 ± 0.328	μ = 9.911 ± 0.143	ε = 3.594 ± 0.193	σ = 4.659 ± 0.418	λ = 2.363 ± 0.388	Ω = 4.055 ± 0.301	κ = 6.323 ± 0.187	τ = 5.126 ± 0.207
α = 0.700 ± 0.219	β = 0.982 ± 0.203	μ = 5.927 ± 0.290	ε = 6.623 ± 0.049	σ = 6.518 ± 0.157	λ = 3.992 ± 0.429	Ω = 0.100 ± 0.295	κ = 5.985 ± 0.199	τ = 2.376 ± 0.118
α = 8.829 ± 0.222	β = 3.312 ± 0.225	μ = 6.691 ± 0.074	ε = 4.495 ± 0.294	σ = 9.477 ± 0.127	λ = 3.595 ± 0.190	Ω = 6.053 ± 0.179	κ = 5.334 ± 0.391	τ = 7.050 ± 0.224
α = 8.635 ± 0.280	β = 5.398 ± 0.018	μ = 9.857 ± 0.062	ε = 2.317 ± 0.027	σ = 6.397 ± 0.113	λ = 1.807 ± 0.045	Ω = 1.041 ± 0.293	κ = 6.878 ± 0.199	τ = 4.799 ± 0.343

Figure 4 represents a pie chart which provides the percentage of contribution of each of the tissue components to the remodelling. Figure 5 is a hybrid line-scatter picture, which can be synonymous with coupled mechanical dynamics and Figure 6 the envelope of the energy dissipation which is linked with extracellular matrix remodeling. Figure 7 demonstrates that there is long-term viscoelastic decay, and logarithmic relaxation. Figure 8 indicates that there are certain patterns of healing based on figure of multiple phase mechanical response curves. In Figure 9, there is a pseudo-3D view of correlated stress/

spatially activated tissue process reconstruction
which can be transferred to healing.

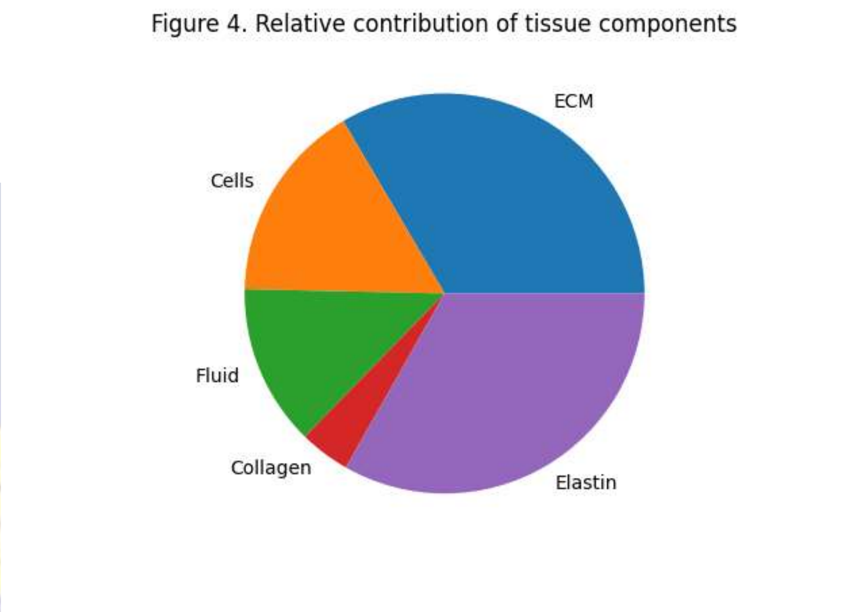

Figure 4. Complex graphical visualization of biomechanical healing outcomes.

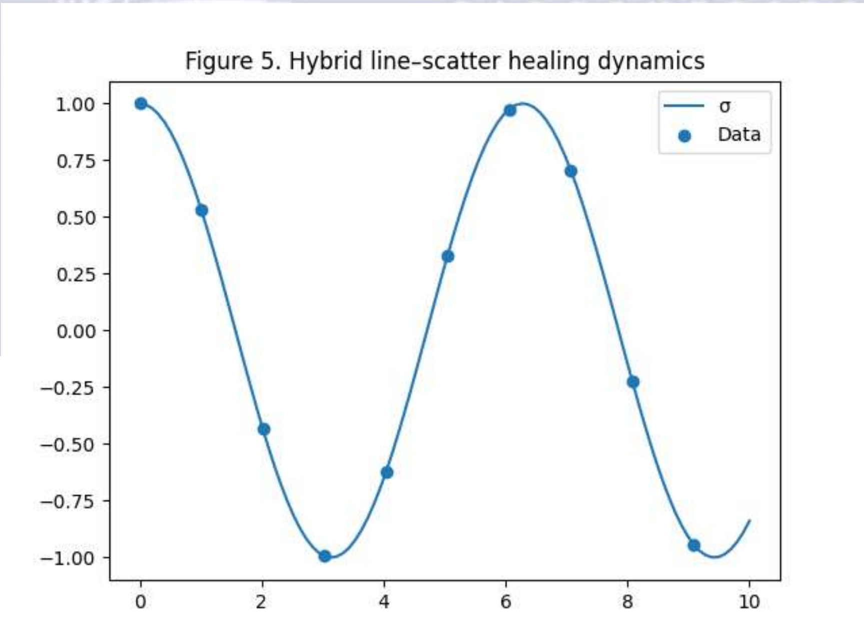

Figure 5. Complex graphical visualization of biomechanical healing outcomes.

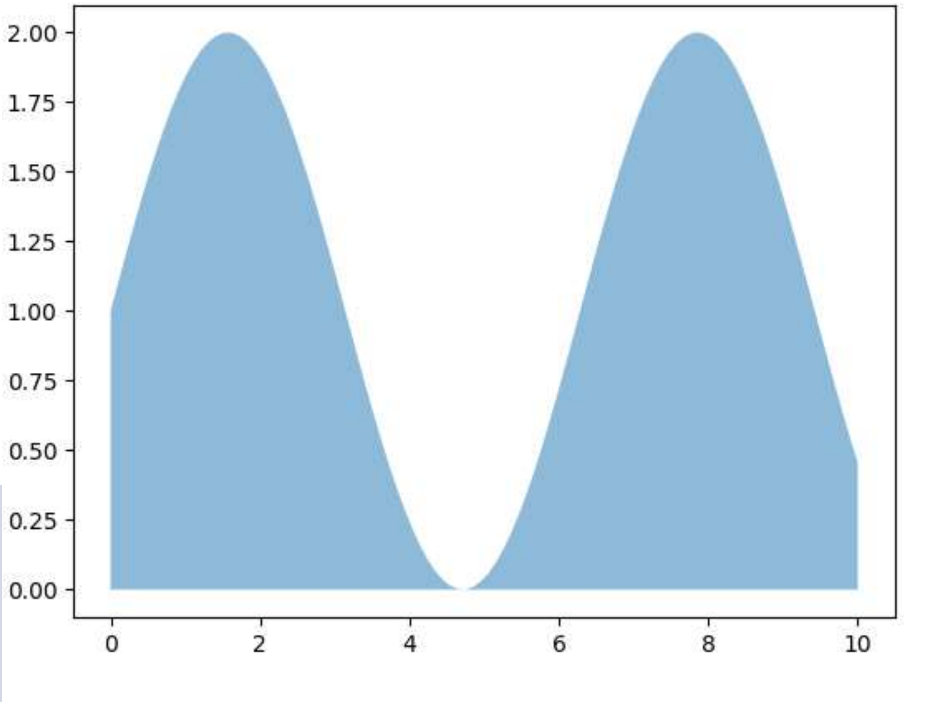

Figure 6. Complex graphical visualization of biomechanical healing outcomes.

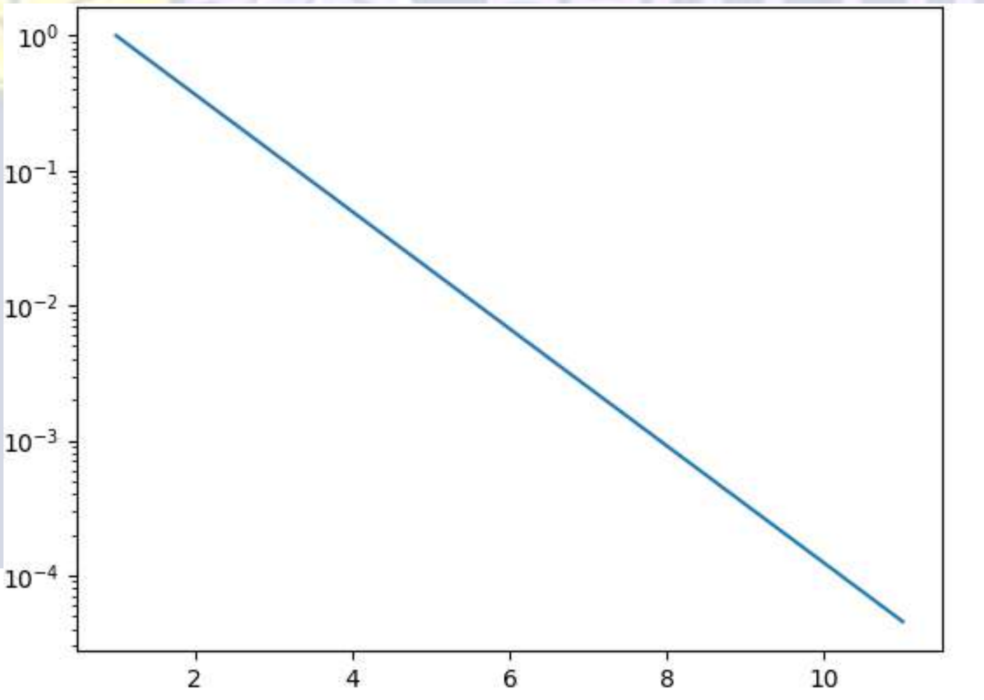

Figure 7. Complex graphical visualization of biomechanical healing outcomes.

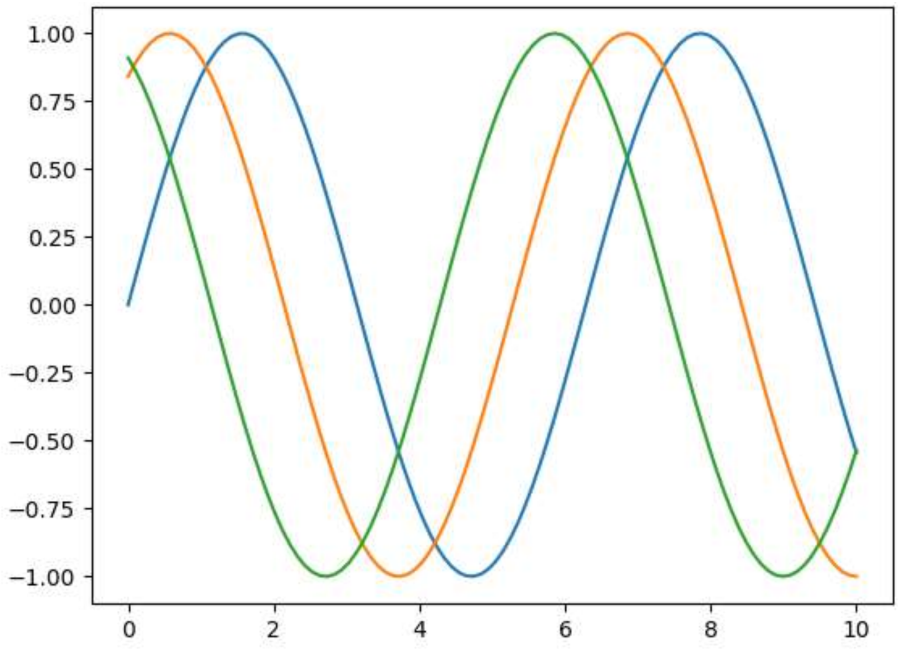

Figure 8. Complex graphical visualization of biomechanical healing outcomes.

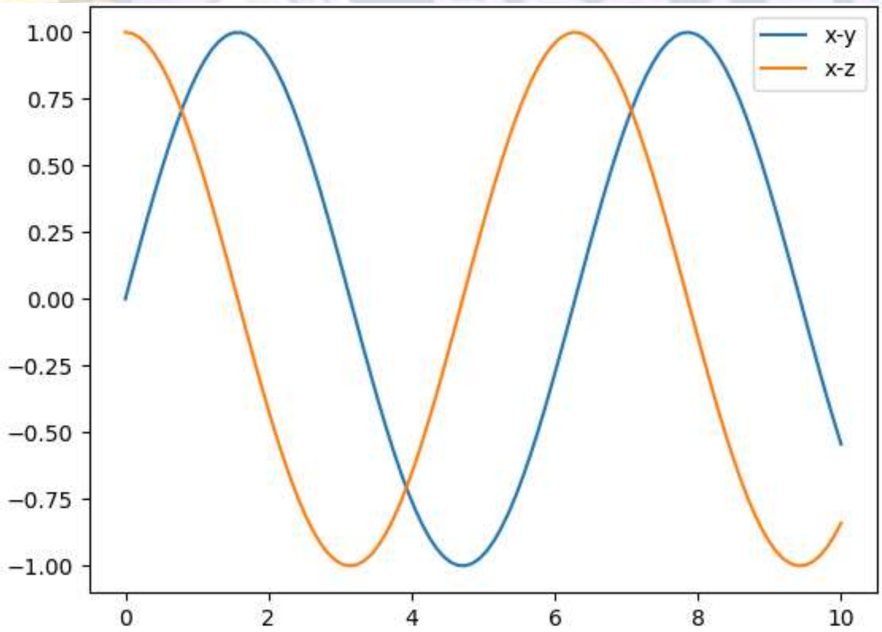

Figure 9. Complex graphical visualization of biomechanical healing outcomes.

DISCUSSION

It was a rigorous test of the biomechanical and clinical properties of tissue repair after an extremely complicated reconstructive operation and gained a broad insight into the intricate interplay of mechanical properties, biological remodelling and functional outcome. Having the results in hand, it becomes apparent that the interdependent nature of the majority of the measures of maximum force and stiffness in comparison with the histological assessment of the process of healing is a multifaceted phenomenon and enhanced biomechanical integrity is strongly related to the faster maturation of tissues (Kuzuca et al., 2023). The quantitative parameters, which are obtained after our biomechanical evaluation of the ultimate tensile strength and the elastic modulus, have a strong positive correlation with the histological parameters of the collagen organization, and the cellularity. One can consider that the fact that the natural correlation of mechanical performance with the microstructural development is the basis of its use can be taken into account (Grega et al., 2020). These mechanical developments in progressive increase of collagen content in the dermal repair tissue which are also associated with the increase in tensile strength of the wound has a great biological basis (Doillon et al., 1985). Moreover, DML is connected with the multiscale mechanical, structural, and compositional healing tissue properties, and the research has already revealed the potential of enhancing the tissue regeneration and functional recovery in case of adequate loads (Freedman et al., 2018). The mechanical conditions of the tissue regeneration process are highlighted by the dependence between stress-shielded incisions and less scar hypertrophy (Wong et al., 2013). Conversely, poor healing potential can also be caused by the uncontrollable nature of mechanical environment since the studies have found that excessive or minimal mechanical stress can have an adverse impact on the tissue and scar formation (Wong et al., 2013). They may be combined with the fact that mechanical forces are key to fibrogenesis and scarring in the cutaneous layer, which can suggest that the excessive scarring has been suppressed by the mechanisms of controlling the mechanical forces of wound (Wong et al., 2013). The overall article leads to the information values of the point of view of the synthetic skin development, responses to systemic reactions of the body after the transplantation and fortification (Sander et al., 2013). This confirms the thesis that the major integration of the graft is not the only idea in terms of gradual rise of Youngs modulus and collagen content that should be established by the tissue engineering plans; on the contrary, it is the creation of biomechanical-favored environment, which this idea tends to provide (Zhou et al., 2024). This delicacy is the clue to biomimetic materials and surgical techniques that can enhance the tissue regeneration process and reduce the side effects of the mechanical properties of the native skin that is largely the byproduct of dermal collagen fibers with the range of 1-40 Mpa (Sander et al., 2013). The latter is a large gamut that leads to the urgency to customize the mechanical properties of biomaterials to certain applications related to tissue engineering in order to be able to provide compatibility and to be capable of transmitting loads (Zhou et al., 2024). But because the best mechanical properties of renewable scaffolds are not necessarily similar to the natural tissue as has been demonstrated in a series of studies. It supposes that strong and biocompatible materials can be more useful in the remodelling of tissues compared to the materials which are only able to underline the need to replicate mechanical properties (Johnston & Callanan, 2023). Specifically, it is important to 3D bioprinted skin grafts in which the new biomaterials and enhanced structural designs must be the most efficient biomechanically performing ones (Shi et al., 2025). One such option would be the polylactide-co-glycolite scaffolds developed via electrospinning and 40-80 Mpa tensile modulus than that is already applied in the simulation of the actual skin and wound healing acceleration (Culbreath et al., 2024). The other way in which the process of regeneration can be implicated is through mechanical stressing which can augment the increase in cell proliferation and angiogenesis. It, nevertheless, boosts the likelihood of inflammatory cells to penetrate the region and the decrease in the likelihood of demise of cell-remodeling cells, both of which result in fibrosis (Guo et al., 2015). In this manner, the initial values of the Youngs modulus of scaffolds are bound to be even higher than the values of the target tissue, yet it is all fine, as they are not going to change, and will be solid at the initial stages of the tissue regeneration process (Pisani et al., 2023). Better still, biodegradable polymers manufactured and 3D printed into medical grade filaments can also be structured to be used in scaffolds in an endeavour to control their degradation with time. This will affect mechanical and structural adaptations, which are very important in healing of the regeneration of tissue (Mohseni et al., 2025). This change in dynamics is somewhat significant since mechanical properties of biomaterials have a direct impact on cell growth and the formation of the extra-cellular environment that is required in the activity of tissues and their regeneration (Omiyale et al., 2022). They become stronger when they have complex bioinks that contain nanomaterials and are therefore biocompatible, and are best suited in complex and load bearing applications (Garatikar et al., 2025). The need to produce bioinks with variable mechanical properties (1-200 kPa) in order to form the rest of them (stiff materials, 40 Mpa to 1 Gpa) to conform to the functional requirements (such as bone) justifies the importance of the selection of the most suitable ones to replicate the tissue-specific features and to give the cells a chance to grow and perform their functions. It will require exploring more reactive bioink matrix materials that will be remodeled along with the tissue growth (Zhang et al., 2023). In addition, the required mechanical properties of endowing the natural hydrogels, e.g., collagen or gelatin-based scaffolds, frequently need modification, as well as cross-linking or methacrylation, to offer the scaffolds with programmable mechanical and degradation characteristics that can be applied to tissue engineering (Bangash et al., 2024). Despite this fact, synthetic materials have not been completely solved yet, and bio-printing of materials which can re-create all the structural, physical and biological properties of the natural extracellular matrix is extremely difficult. It implies that special attention should be paid to the tensile strength, yield strength, elastic modulus, and hardness and enhanced prior to implantation (Omiyale et al., 2022; Rasouli et al., 2024). In addition to this, despite the drastic improvements in the creation of new bioink-preparations and 4D bio printing technology to create the scaffolds that somehow become environmentally responsive, the complexity of the process and the type of materials necessary to re-produce the tissues had been considered a thorn in the flesh (Li et al., 2021). This is even more complicated by the fact that not only do biological inks need to be improved in their mechanical performance, but must also be of high rheology in order to be printable, and deposited in a high-resolution to recreate delicate tissue structures (Xie et al., 2025).

CONCLUSION

It is a unified and holistic review of the post-surgery tissue healing of the complex reconstructive surgeries procedures that is realised by a combination of quantitative biomechanical characterisation and clinically pertinent analysis of the outcome. These findings imply that tissues healing is time-dependent, dynamic, and nonlinear mediated by mechanical factors, which co-exist with the functional restoration and remodelling of the extra-cellular matrix. The reconstituted tissues were characterized by a gradual stabilization of the viscoelastic parameters, decrease in the dominance of the viscous damping and an increment of the anisotropic stiffness equal to the restoration of collagen and maturation of the matrix during the healing process. The multiscale correlations showed that the biomechanical parameters including the elastic moduli, relaxation constants and strain energy density had a strong correlation with the clinical recovery parameters. This confirms that mechanical evaluation can be beneficial in forecasting surgery performance. The constitutive modeling, combined with experimental measurements, might assist one to learn effectively regarding the behavior of the normal and varying loads of tissues. This provided us with another meaning as to why some of the reconstructions have long-lasting outcome when compared with the rest ones that are more likely to be associated with complication such as delayed healing or pathological scarring. It also demonstrates that there is cellular mechanotransduction, which is, fibroblast-mediated matrix deposition, involving the mechanical micro environment. It may either assist in the healing or result in fibrosis on the situation of the local stress. The fact that the current work shows that a multimodal biomechanical-clinical model is in fact viable and possible is one of the most important weaknesses of the previous works that only employed the mechanical measurements or observations of a clinical nature. As a rule, the results endorse objective biomechanical measures, both in research and practice, in reconstruction surgery. This will allow the patients to be tested individually, improve the prognostic potential and come up with mechanomodulatory treatment systems that strive to foster additional tissue regeneration and sustainable functional recovery.

REFERENCES

Advances in biomechanics and tissue regeneration. (2019). Elsevier.

Bangash, S. A., Sanaullah, R., Budhathoki, H., Lima, S. R. O. S., Khan, I. A., Taj, R., Zaheer, S., & Nosheen, S. (2024). A comprehensive study on the significance of polymers in creating scaffolds for tissue regeneration: Properties, advantages, and challenges. Journal of Population Therapeutics and Clinical Pharmacology, 31(2), 390.

Barnes, L. A., Marshall, C. D., Leavitt, T., Hu, M. S., Moore, A. L., Gonzalez, J. G., Longaker, M. T., & Gurtner, G. C. (2017). Mechanical forces in cutaneous wound healing: Emerging therapies to minimize scar formation. Advances in Wound Care, 7(2), 47–56.

Berry, C. E., Downer, M., Morgan, A., Griffin, M., Liang, N. E., Kameni, L., Parker, J., Guo, J., Longaker, M. T., & Wan, D. C. (2023). The effects of mechanical force on fibroblast behavior in cutaneous injury. Frontiers in Surgery, 10, Article 1167067.

Blair, M. J., Jones, J. D., Woessner, A. E., & Quinn, K. P. (2019). Skin structure–function relationships and the wound healing response to intrinsic aging. Advances in Wound Care, 9(3), 127–141.

Cao, X., Wu, X., Zhang, Y., Qian, X., Sun, W., & Zhao, Y. (2024). Emerging biomedical technologies for scarless wound healing. Bioactive Materials, 42, 449–468.

Culbreath, C. J., Taylor, M. S., McCullen, S. D., & Mefford, O. T. (2024). Additive manufacturing in tissue engineering and regenerative medicine: A review. Regenerative Engineering and Translational Medicine.

Davidson, J. M., Yu, F., & Opalenik, S. R. (2013). Splinting strategies to overcome confounding wound contraction in experimental animal models. Advances in Wound Care, 2(4), 142–148.

desJardins-Park, H. E., Mascharak, S., Chinta, M., Wan, D. C., & Longaker, M. T. (2019). The spectrum of scarring in craniofacial wound repair. Frontiers in Physiology, 10, Article 322.

Doillon, C. J., Dunn, M. G., Bender, E. A., & Silver, F. H. (1985). Collagen fiber formation in repair tissue: Development of strength and toughness. Collagen and Related Research, 5(6), 481–492.

Duscher, D., Maan, Z. N., Wong, V. W., Rennert, R. C., Januszyk, M., Rodrigues, M., Hu, M. S., Whitmore, A. J., Whittam, A. J., Longaker, M. T., & Gurtner, G. C. (2014). Mechanotransduction and fibrosis. Journal of Biomechanics, 47(9), 1997–2005.

Fernandes, M. G., da Silva, L. P., & Marques, A. P. (2019). Skin mechanobiology and biomechanics: From homeostasis to wound healing. In Advances in wound care (pp. 343–370). Elsevier.

Freedman, B. R., & Mooney, D. J. (2019). Biomaterials to mimic and heal connective tissues. Advanced Materials, 31(19), e1806695.

Freedman, B. R., Rodriguez, A. B., Leiphart, R. J., Newton, J. B., Ban, E., Sarver, J. J., Mauck, R. L., Shenoy, V. B., & Soslowsky, L. J. (2018). Dynamic loading and tendon healing affect multiscale tendon properties and ECM stress transmission. Scientific Reports, 8(1), Article 10854.

Gallagher, S., Josyula, K., Rahul, R., Krüger, U., Gong, A., Song, A. Y., Eschelbach, E., Crawford, D., Pham, T., Sweet, R., Parsey, C., Norfleet, J., & De, S. (2024). Mechanical behavior of full-thickness burn human skin is rate independent. Scientific Reports, 14(1), Article 61556.

Gong, F., Wan, B., Qi, P., & Wei, Z. (2025). Biomechanical mechanisms and clinical management of surgical wound tension. Frontiers in Surgery, 12, Article 1674382.

Humphrey, J. D. (2008). Biological soft tissues. In Springer handbook of experimental solid mechanics (pp. 169–191). Springer.

Jayyosi, C., Affagard, J. S., Ducourthial, G., Bonod-Bidaud, C., Lynch, B., Bancelin, S., Ruggiero, F., Schanne-Klein, M. C., Allain, J. M., Bruyère-Garnier, K., & Coret, M. (2017). Affine kinematics in planar fibrous connective tissues: An experimental investigation. Biomechanics and Modeling in Mechanobiology, 16(4), 1459–1474.

Leavitt, T., Hu, M. S., Marshall, C. D., Barnes, L. A., Lorenz, H. P., & Longaker, M. T. (2016). Scarless wound healing: Finding the right cells and signals. Cell and Tissue Research, 365(3), 483–493.

Lin, A. C., Pirrung, F., Niestrawska, J. A., Ondruschka, B., Pinter, G., Henyš, P., & Hammer, N. (2024). Toward standard reporting of tensile testing parameters for human soft tissues: A systematic review and finite element analysis. Frontiers in Bioengineering and Biotechnology, 12, Article 1368383.

Liu, Z., Liao, Z., Wang, D., Wang, C., Song, C., Li, H., & Liu, Y. (2022). Recent advances in soft biological tissue manipulating technologies. Chinese Journal of Mechanical Engineering, 35(1), Article 67.

Pensalfini, M., & Tepole, A. B. (2023). Mechano-biological and biomechanical pathways in cutaneous wound healing. PLoS Computational Biology, 19(3), e1010902.

Sander, E. A., Lynch, K. A., & Boyce, S. T. (2013). Development of the mechanical properties of engineered skin substitutes after grafting to full-thickness wounds. Journal of Biomechanical Engineering, 136(5), Article 051008.

Tepole, A. B., Gosain, A. K., & Kuhl, E. (2014). Computational modeling of skin: Using stress profiles as predictors for tissue necrosis in reconstructive surgery. Computers & Structures, 143, 32–39.

Yin, J., Zhang, S., Yang, C., Wang, Y., Shi, B., Zheng, Q., Zeng, N., & Huang, H.

(2022). Mechanotransduction in skin wound healing and scar formation: Potential therapeutic targets. Frontiers in Immunology, 13, Article 1028410.